High-frequency Alfvén waves in multi-ion coronal plasma: Observational implications

L. Ofman,[1,2] J. M. Davila,[3] V. M. Nakariakov,[4] and A.-F. Viñas[5]

Received 9 December 2004; revised 18 March 2005; accepted 29 April 2005; published 9 September 2005.

[1] We investigate the effects of high-frequency (of order ion gyrofrequency) Alfvén and ion-cyclotron waves on ion emission lines by studying the dispersion of these waves in a multi-ion coronal plasma. For this purpose we solve the dispersion relation of the linearized multifluid and Vlasov equations in a magnetized multi-ion plasma with coronal abundances of heavy ions. We also calculate the dispersion relation using nonlinear one-dimensional hybrid kinetic simulations of the multi-ion plasma. When heavy ions are present the dispersion relation of parallel propagating Alfvén cyclotron waves exhibits the following branches (in the positive $\Omega - k$ quadrant): right-hand polarized nonresonant and left-hand polarized resonant branch for protons and each ion. We calculate the ratio of ion to proton velocities perpendicular to the direction of the magnetic field for each wave modes for typical coronal parameters and find strong enhancement of the heavy ion perpendicular fluid velocity compared with proton perpendicular fluid velocity. The linear multifluid cold plasma results agree with linear warm plasma Vlasov results and with the nonlinear hybrid simulation model results. In view of our findings we discuss how the observed nonthermal line broadening of minor ions in coronal holes may relate to the high-frequency wave motions.

Citation: Ofman, L., J. M. Davila, V. M. Nakariakov, and A. F. Viñas (2005), High-frequency Alfvén waves in multi-ion coronal plasma: Observational implications, *J. Geophys. Res.*, *110*, A09102, doi:10.1029/2004JA010969.

1. Introduction

[2] The observation of minor ion emission lines in EUV in the solar corona has been the major diagnostic tool of coronal physical properties, such as temperature and density, for the past several decades. The launch of spectroscopic EUV instruments on sounding rockets [*Hassler et al.*, 1990; *Neupert et al.*, 1992; *Davila et al.*, 1997] and Ultraviolet Coronagraph Spectrometer (UVCS) [*Kohl et al.*, 1995], Coronal Diagnostic Spectrometer (CDS) [*Harrison et al.*, 1995], and Solar Ultraviolet Measurement of Emitted Radiation (SUMER) [*Wilhelm et al.*, 1995] on the Solar and Heliospheric Observatory (SOHO) further increased the use on these remote sensing tools as one of the major coronal observation methods. Ground-based observations of coronal lines in the visible spectrum were also obtained [e.g., *Hara and Ichimoto*, 1999].

[3] The observed emission lines have finite width in wavelength due to the Doppler effect of the emitting ion motion along the line of sight (i.e., $\Delta\lambda/\lambda \approx v/c$, where $\Delta\lambda$ is the Doppler shift at wavelength λ, v is the corresponding velocity of the emitting ion, and c is the speed of light) and due to instrumental effects [e.g., see *Withbroe et al.*, 1982; *Kohl and Withbroe*, 1982]. The Doppler broadening due to Maxwellian velocity distribution of the ions leads to Gaussian emission line profile with a $1/e$ width that corresponds to twice the thermal speed of the ions, $v_{th,i} = \sqrt{2k_B T_i/m_i}$. Thus the observed line is usually separated in two parts: thermal and nonthermal. The temperature and the corresponding thermal velocity can be determined independently, for example, from emission line intensity ratio of two ions. The nonthermal motions can be obtained by subtracting the thermal Gaussian profile from the observed emission line profile. The nonthermal motions may contain microscopic non-Maxwellian kinetic motions of the emitting ions and unresolved macroscopic bulk motion of the plasma due to waves or turbulence. If both thermal and nonthermal motions have Gaussian distribution, then the observed $1/e$ ion emission line width square is the sum of squares of the thermal and nonthermal widths (i.e., in terms of velocities $v_{1/e}^2 = v_{th,i}^2 + \xi^2$, where ξ is the rms nonthermal velocity). Evidently, the relation of the observed line emission to the actual physical properties and motions of the plasma depends strongly on the assumptions and the modeling used in the reduction of the observations and on the correction for the instrumental effects [*Kohl et al.*, 1997; *Ofman and Davila*, 1997, 2001].

[4] The detection of unresolved plasma motions at the base of the corona, such as Alfvén waves or turbulence, is

[1]Department of Physics, Catholic University of America, Washington, DC, USA.
[2]Also at NASA Goddard Space Flight Center, Code 612.1, Greenbelt, Maryland, USA.
[3]NASA Goddard Space Flight Center, Code 612.1, Greenbelt, Maryland, USA.
[4]Physics Department, University of Warwick, Coventry, UK.
[5]NASA Goddard Space Flight Center, Code 612.2, Greenbelt, Maryland, USA.

0148-0227/05/2004JA010969$09.00

an important goal for the understanding of the heating of the corona, and the acceleration of the solar wind since these waves and motions are the main "ingredients" in many recent coronal heating and solar wind acceleration models [*Marsch and Tu*, 1997; *Tu and Marsch*, 1997; *Ofman and Davila*, 1998; *Nakariakov et al.*, 2000; *Ofman and Davila*, 2001; *Cranmer*, 2002; *Dmitruk et al.*, 2002; *Hollweg and Isenberg*, 2002; *Ofman*, 2004; *Cranmer and van Ballegooijen*, 2003; *Li*, 2003; *Vainio et al.*, 2003; *Li et al.*, 2004; *Isenberg*, 2004, and references therein]. The observed nonthermal broadening of minor ion emission lines in various locations in the solar corona provide the constraints for possible presence of Alfvén waves or turbulent fluctuation spectra [*Ofman and Davila*, 1997; *Narain et al.*, 2001; *Pekünlü et al.*, 2002; *O'Shea et al.*, 2003]. However, these studies considered Alfvén waves in the MHD regime where the response of heavy ions to wave motions is practically identical to protons.

[5] Since the corona is nearly collisionless beyond $2-3R_\odot$ (i.e., the collision frequency is smaller than the relevant wave frequency) and weakly collisional close to the Sun, the wave motions of the minor ions in the corona may be in principle different then the proton and electron wave motions. In particular waves with frequencies near and above ion gyrofrequencies, which is significantly above the typical collision frequency in the corona, can affect heavy ions in dramatically different ways than protons. As shown in this paper, the difference in velocity depends on the charge to mass ratio, the abundance of the ions relative to protons, and on the ion temperatures. Therefore determination of the ion thermal and nonthermal motions from observed line widths requires taking high-frequency wave motions into account.

[6] Propagation of Alfvén waves in a multi-ion plasmas have been considered in the past using Vlasov's collisionless theory [e.g., see *Smith and Brice*, 1964; *Gendrin and Roux*, 1980; *Gomberoff and Elgueta*, 1991]. Multifluid equations for Maxwellian plasma that consists of interacting electron, proton, and heavy ions fluids are well applicable to the lower solar corona and produce similar results. The dispersion relation (real frequency versus wave number) obtained with the multifluid equations in the cold plasma approximation is similar to the dispersion relation obtained from the more complex collisionless Vlasov equations.

[7] Recently, two-dimensional three fluid model of the fast solar wind driven by Alfvén waves was developed [*Ofman and Davila*, 2001; *Ofman*, 2004]. *Ofman* [2004] investigated the acceleration of the fast solar wind in coronal holes with a spectrum of low-frequency Alfvén waves ($\omega \ll \Omega_i$) by solving numerically the nonlinear, time-dependent, three-fluid equations in two dimensions. The three fluids were electrons, protons, and O^{5+} or He^{++} ions. The heating of the solar wind plasma due to dissipation of the low-frequency MHD waves by hyperviscosity and hyperresistivity, in addition to an empirical heat input term, was investigated.

[8] *Ofman and Davila* [2001] and *Ofman* [2004] found that nonthermal motions due to low-frequency Alfvén waves with amplitudes constrained by observations in the lower corona can explain the nonthermal line broadening of hydrogen (Ly-α) emission lines in coronal holes observed by UVCS [*Kohl et al.*, 1995], but these waves cannot account for the broad emission lines of O^{5+} ions. Motivated by temperature anisotropy deduced from observations of O^{5+} ion line emission and the Doppler dimming effect [*Kohl et al.*, 1998; *Li et al.*, 1998], it has been suggested that the broad emission lines are due to perpendicular heating by ion cyclotron waves [*Cranmer et al.*, 1999; *Marsch*, 1999]. Ion-cyclotron waves were suggested as the heating mechanism for coronal plasma ions in the past [*Dusenbery and Hollweg*, 1981; *McKenzie and Marsch*, 1982; *Isenberg and Hollweg*, 1982; *Axford and McKenzie*, 1992] and were extensively studied in this context using linear Vlasov, quasilinear, and nonlinear kinetic simulation methods (see the review by *Hollweg and Isenberg* [2002]). In this study we are not concerned with heating by these waves but with the possible contribution of high-frequency Alfvén cyclotron waves to perpendicular ion motions.

[9] Recently, one-dimensional (1-D) hybrid simulations were used to study proton-He^{++}-O^{5+} plasma in the solar wind [*Xie et al.*, 2004]. In the hybrid model the electrons are treated as fluid and the ions are described kinetically [e.g., *Winske and Omidi*, 1993]. In the work of *Xie et al.* [2004] a driving spectrum of ion-cyclotron waves was included and in some cases a relative drift between the heavy ions and protons and good qualitative agreement with Vlasov dispersion relation was found. However, owing to numerical reasons, the abundance of the O^{5+} was unrealistically high. In this study we include the more abundant O^{6+} ion in addition to protons and He^{++} and do not include ion drift (note that $n_{O^{6+}}/n_{O^{5+}} \approx 150$ [*Wimmer-Schweingruber et al.*, 1998]).

[10] The present study is focused on the dispersion properties of Alfvén cyclotron waves and their observational implication. Here, we use the linearized multifluid equations for cold multi-ion plasma, Vlasov dispersion relation for warm multi-ion plasma, and 1-D hybrid kinetic model of warm multi-ion plasma to explore the effects of high-frequency waves of the order of the ion gyrofrequency on the dispersion and motion of the heavy ions and discuss their observational implications. We include the two most abundant heavy ions, He^{++} and O^{6+}, with their typical coronal abundances in the models, and consider the typical plasma β (ratio of thermal to magnetic pressure) in the lower corona.

[11] In section 2 we present the linear multifluid cold plasma model, in section 3 we present the multifluid dispersion relations, in section 4 we show the relation between ion and proton fluid velocities, in section 5 we show the solution of the Vlasov dispersion relation for warm multicomponent plasma, in section 6 we present the dispersion relation obtained from the hybrid kinetic model of the warm multi-ion plasma, and section 7 is devoted to discussion of the observational implications and to conclusions.

2. Linearized Multifluid Equations

[12] Assuming that the characteristic spatial scales of the inhomogeneity are much larger than the relevant wavelengths, we consider Alfvén and ion-cyclotron waves in a homogeneous multifluid cold plasma which consists of electrons, protons, and heavy positive ions of the electric charge $q_i = Z_i e$ and mass $m_i = A_i m_p$. Gravity, pressure gradients, electron inertia, and dissipation are neglected in

this study. We assume quasi-neutrality and neglect the displacement current. Also, we study linear perturbations only (i.e., $|V| \ll C_A$, where C_A is the Alfvén speed defined below). Owing to the effects of Coulomb friction in the lower corona ($r < 2R_\odot$) the drift of heavy ions relative to protons is small compared with the Alfvén speed, and we neglect it in this study. This is confirmed by the 2-D three-fluid model of the fast solar wind in coronal holes that includes Coulomb friction terms [*Ofman*, 2004]. The model calculations show that the relative drift between protons and heavy ions is negligible for $r < 2R_\odot$ [see *Ofman*, 2004, Figure 10]. In addition, according to UVCS observation [*Kohl et al.*, 1998], the O^{5+} drift below $1.9R_\odot$ may be negligible, and therefore the O^{6+} ion which is more abundant by two orders of magnitude than O^{5+} ion is unlikely to drift considerably relative to protons due to Coulomb friction. The governing equations are the equations of motions for protons,

$$\frac{\partial \mathbf{V}_p}{\partial t} = \frac{e}{m_p c}\left(\mathbf{V}_p - \mathbf{V}_e\right) \times \mathbf{B}_0, \tag{1}$$

and for each heavy ion,

$$\frac{\partial \mathbf{V}_i}{\partial t} = \frac{Z_i e}{m_i c}(\mathbf{V}_i - \mathbf{V}_e) \times \mathbf{B}_0, \tag{2}$$

and the magnetic induction equation,

$$\frac{\partial \mathbf{B}}{\partial t} = \nabla \times (\mathbf{V}_e \times \mathbf{B}_0), \tag{3}$$

where $\mathbf{V}_p$ is the velocity of protons and $\mathbf{V}_i$ is the velocity of ions (in this study we set $i = He^{++}$, O^{6+}), β_0 is the background magnetic field, and the electron velocity is given by

$$\mathbf{V}_e = \sum_i Z_i \frac{n_i}{n_e}\mathbf{V}_i + \frac{n_p}{n_e}\mathbf{V}_p - \frac{c}{4\pi e n_e}\nabla \times \mathbf{B}, \tag{4}$$

where $\mathbf{B}$ is the perturbed magnetic field and n_p, n_i, and n_e denote proton, ion, and electron number densities, respectively. As we consider waves with frequencies significantly below the electron plasma frequency, the quasi-neutrality condition implies that electron charge density is equal to the sum of the proton and positive ion charge densities,

$$n_e = n_p + \sum_i Z_i n_i. \tag{5}$$

In equations (1)–(5), ions and protons interact with each other electromagnetically, through the perturbations of the field and the charge neutrality condition. Since we neglected pressure gradients and the Alfvén waves are incompressible, we do not need to solve the equations of continuity.

[13] In the following, we assume that the unperturbed magnetic field is directed along the z-axis and consider transverse waves propagating parallel to the field, which perturb the x and y components of the velocity vectors and the magnetic field propagating parallel to the field only. Also, we assume the harmonic dependence of the perturbed quantities upon time and the longitudinal coordinate, $\propto \exp(i\omega t - ikz)$.

3. Multifluid Dispersion Relation

[14] It is convenient to consider left-hand and right-hand circularly polarized transverse waves, thus introducing the following variables [e.g., see *Stix*, 1992]:

$$V_{p\pm} = V_{px} \pm iV_{py}, \quad V_{i\pm} = V_{ix} \pm iV_{iy},$$
$$V_{e\pm} = V_{ex} \pm iV_{ey}, \quad B_\pm = B_x \pm iB_y. \tag{6}$$

With the use of these variables, equations (1)–(4) can be rewritten as

$$\omega V_{p\pm} = \mp\Omega_p\left(V_{p\pm} - V_{e\pm}\right), \tag{7}$$

$$\omega V_{i\pm} = \mp\Omega_i(V_{i\pm} - V_{e\pm}), \tag{8}$$

$$\omega B_\pm = -kB_0 V_{e\pm}, \tag{9}$$

$$V_{e\pm} = \sum_i \frac{Z_i n_i}{n_e} V_{i\pm} + \frac{n_p}{n_e} V_{p\pm} \mp \frac{kc}{4\pi e n_e} B_\pm, \tag{10}$$

where

$$\Omega_p = \frac{eB_0}{m_p c}, \quad \Omega_i = \frac{Z_i e B_0}{m_i c} \tag{11}$$

are the proton and ion cyclotron frequencies, respectively. The consistency condition gives us the dispersion relation for the transverse parallel waves in multi-ion plasma [e.g., see *Smith and Brice*, 1964],

$$1 \mp \frac{C_A^2 k^2}{\Omega_p \omega} - \sum_i \frac{f_i \Omega_i}{\Omega_i \pm \omega} - \frac{\left(1 - \sum_i f_i\right)\Omega_p}{\Omega_p \pm \omega} = 0, \tag{12}$$

where

$$C_A = \frac{B_0}{\left(4\pi m_p n_e\right)^{1/2}} \tag{13}$$

is the convenient definition of the Alfvén speed (which reduces to the single fluid Alfvén speed in the absence of heavy ions) and

$$f_i = \frac{Z_i n_i}{n_e} \tag{14}$$

is the relative heavy ion charge density. For the solar coronal conditions, the typical value of the parameter f_i is 0.1 for He^{++} and 4.8×10^{-3} for O^{6+}.

[15] In the low-frequency limit, dispersion relations (12) contain two small parameters, the ratios ω/Ω_p and ω/Ω_i. As the MHD limit is approached, both ratios tend to zero and may be considered of the same order. Expanding up to the

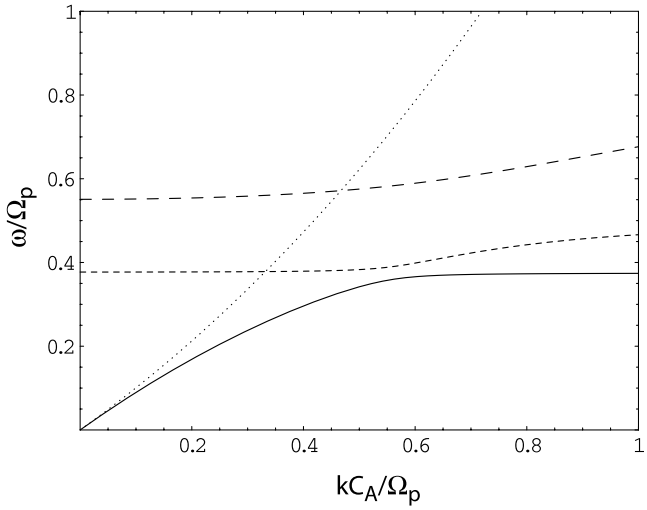

Figure 1. The solution of the four-fluid Alfvén wave dispersion relation with typical coronal parameters of electron, proton, He^{++}, and O^{6+} plasma. The solid and dashed curves corresponds to the left-hand circularly polarized waves, which experience proton and ion cyclotron resonances. The dotted curve correspond to the right-hand polarized waves.

quadratic terms of the ratios the denominators of the third and the fourth terms of the dispersion relation and assuming that one heavy ion is present, we obtain

$$\omega^2 - C_A^2 k^2 \mp \frac{\omega^3}{\Omega_p} + f_i \omega^2 \left[\left(\frac{\Omega_p}{\Omega_i} - 1 \right) \mp \frac{\omega}{\Omega_p} \left(\frac{\Omega_p^2}{\Omega_i^2} - 1 \right) \right] = 0. \tag{15}$$

[16] In the absence of the heavy ions (f_i = 0), the dispersion relation reduces to

$$\omega^2 - C_A^2 k^2 \mp \frac{\omega^3}{\Omega_p} = 0. \tag{16}$$

Taking into account that $\omega \approx C_A k$, the third term may be rewritten as $C_A^3 k^3/\Omega_p$. Note that in the low-frequency limit ($\omega \ll \Omega_p$) equation (16) reduces to the ideal MHD Alfvén wave dispersion relation ($\omega = C_A k$ in the positive $\omega - k$ quadrant).

[17] In the general case, dispersion relation (12) describes resonant dispersive branches for multi-ion plasma. The multifluid cold plasma dispersion is close to the warm plasma Vlasov dispersion relation for the real frequency of the parallel propagating Alfvén waves (see section 5 below). Figure 1 shows the solutions of the dispersion relation for multi-ion plasma with observed coronal abundances of He^{++} ions (f_i = 0.1, Ω_i/Ω_p = 0.5) and O^{6+} (f_i = 4.8×10^{-3}, Ω_i/Ω_p = 0.375). The exact analytical solution of the dispersion relation for the two heavy ions was obtained and plotted with Mathematica©. The sign in equation (12) is selected to show the right-hand and left-hand polarized branches in the positive $\omega - k$ quadrant (the other three quadrants exhibit symmetric and antisymmetric reflections of the branches in this quadrant). The typical feature of this plot is the presence of three resonant branches of the left-hand polarized waves, due to the He^{++} and O^{6+} ions, and proton cyclotron resonances, in addition to one right-hand polarized nonresonant wave, which at high frequencies ($\omega \gg \Omega_p$) becomes the whistler wave.

[18] The dispersion exhibits the well-known frequency gaps, in which no parallel left-hand polarized waves can propagate. The width of frequency gap decreases with the relative (to proton) abundance of the heavy ions [see *Cornwall and Schulz*, 1971; *Cuperman et al.*, 1975; *Isenberg*, 1984; *Cuperman et al.*, 1988]. The dispersion relation was investigated for the three most abundant ions in the solar corona: p, He^{++}, and O^{6+}. The abundance of other minor ions is one to three orders of magnitude smaller than the abundance of O^{6+}, and their effect on the dispersion relation can be neglected for the purpose of this study (the effect of multitude of the coronal ions on ion-cyclotron wave heating was considered by *Cranmer* [2000]).

4. Alfvén Wave Velocity Amplitudes

[19] Consider perturbations of the plasma by the Alfvén and ion-cyclotron waves described by dispersion relation (12). Rewriting equations (7) and (8), we obtain

$$V_{p\pm} = \pm \frac{\Omega_p}{\omega \pm \Omega_p} V_{e\pm}, \tag{17}$$

$$V_{i\pm} = \pm \frac{\Omega_i}{\omega \pm \Omega_i} V_{e\pm}, \tag{18}$$

which allows us to calculate the ratio of the ion and proton linear fluid velocity perturbations induced by Alfvén and ion-cyclotron waves,

$$\frac{V_{i\pm}}{V_{p\pm}} = \frac{\omega/\Omega_p \pm 1}{\omega/\Omega_i \pm 1}. \tag{19}$$

[20] Clearly, in the MHD regime ($\omega \ll \Omega_p, \Omega_i$), equation (19) reduces to the single fluid limit, with $V_{i\pm} = V_{p\pm}$. For higher frequencies, comparable with the resonant frequencies, the frozen-in condition does not apply, and the dynamics of protons and ions becomes very different. This is shown in Figure 2, for the plasma with He^{++} ions (upper panel) and O^{6+} (lower panel) (the ion abundances and other parameters are the same as in Figure 1). Note that the resonant branches are heavily damped for $kC_A/\Omega_p > 1$ in a warm plasma (see section 5 below); therefore we show the dispersion up to $kC_A/\Omega_p = 1$.

[21] In the long wavelength limit ($k \to 0$), one of the roots of dispersion relation (12) tend to the value

$$\omega \to \Omega_i + f_i(\Omega_p - \Omega_i). \tag{20}$$

For this limiting value we get

$$|V_{i\pm}/V_{p\pm}| \to \frac{\Omega_i(1 - f_i)}{\Omega_p f_i} \tag{21}$$

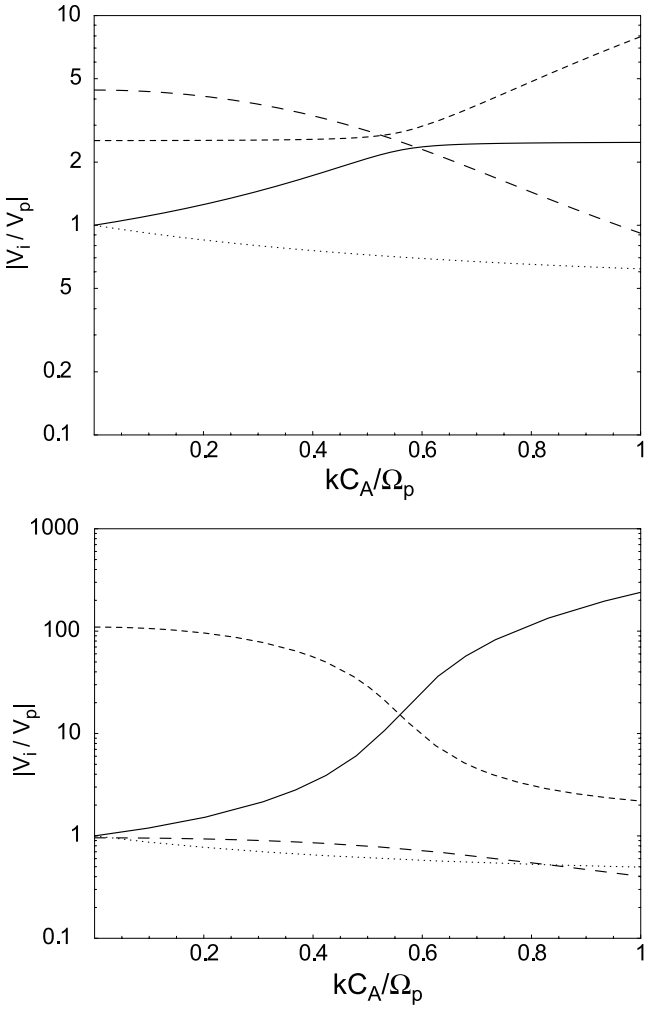

Figure 2. The dependence of the wave velocity amplitude ratio for ions and protons on the normalized wave number (He^{++} in the top panel and O^{6+} in the lower panel). The solid and the dashed curves corresponds to the left hand circularly polarized waves, which experience proton and ion cyclotron resonances. The dotted curves correspond to the right-hand polarized waves.

for the ion-cyclotron branch. For the typical coronal hole parameters used here ($C_A \approx 2000$ km s^{-1}, $\Omega_p = 9.58 \times 10^4$ Rad s^{-1}) this limit is about 4.5 for the He^{++} branch and about 78 for the O^{6+} branch.

[22] It is interesting to note that according to equation (21), the perpendicular velocity amplitude of low-abundance heavy ions ($f_i \rightarrow 0$) in the corona is much larger than proton perpendicular velocity amplitude for this wave mode (see also Figure 2). However, this linear cold plasma result is valid for small velocities $|V_{i\pm}| \ll C_A$ and $|V_{p\pm}| \ll C_A$, and, as evident from the lower panel in Figure 3 below, the damping increases as the abundance decreases. Thus in cases where $|V_{i\pm}/V_{p\pm}| \gg 1$ the linear approximation implies that $|V_{p\pm}| \ll |V_{i\pm}| \ll C_A$ but still allows for proton and ions velocities on the order of several hundred km s^{-1} with typical value of $C_A \approx 2000$ km s^{-1} in the lower corona hole. Below, we show that this result hold in the nonlinear hybrid simulation model.

5. Vlasov Dispersion for Parallel Propagating Electromagnetic Waves in Warm Plasma

[23] To check whether the effect discussed in the previous sections takes place in a realistic low but finite β plasma of the solar corona, we investigate the effects of finite temperature on the dispersion relation of ion-cyclotron waves in the multicomponent plasma by solving numerically the dispersion relation of the linearized Vlasov equation for parallel propagating electromagnetic waves in warm multicomponent plasma. The dispersion relation for isotropic, stationary (i.e., zero drift), multicomponent plasma can be written as [*Scharer and Trivelpiece*, 1967; *Davidson and Ogden*, 1975; *Gary*, 1978, 1993; *Araneda et al.*, 2002]

$$k^2c^2 - \omega^2 - \sum_i \omega_{pi}^2 \left[\frac{\omega}{v_i k}\zeta\left(\frac{\omega \pm \Omega_i}{v_i k}\right)\right] = 0, \qquad (22)$$

where $\omega = \omega_r + i\gamma$ is the complex frequency and k is the wave number along the magnetic field. In the above equation the parallel thermal speed is $v_i = (2k_BT_i/m_i)^{1/2}$, ζ is the plasma dispersion function [*Fried and Conte*, 1961], and the plasma frequency $\omega_{pi} = (4\pi n_i q_i^2/m_i)^{1/2}$. The plasma is assumed to be charge neutral ($\sum_i n_i q_i = 0$) and carry zero current. In the limit of cold plasma ($T \rightarrow 0$) the dispersion relation given by equation (22) approaches the multifluid cold plasma dispersion relation (12).

[24] The solution of Vlasov's dispersion relation (22) for warm plasma with protons, He^{++}, and O^{6+} ions is shown in Figure 3. As discussed above, the relative drift between the protons and ions is small in the lower corona due to the effect of Coulomb friction [*Ofman*, 2004] and was neglected here. Solutions of the Vlasov dispersion relation with drift for proton-He^{++} plasma can be found in the work of *Gomberoff and Elgueta* [1991] and *Xie et al.* [2004].

[25] We have used $n_{He^{++}}/n_p = 0.05$ and $n_{O6+}/n_p = 8 \times 10^{-4}$ with $\beta = 0.01$ (Figure 3a) and $\beta = 0.03$ (Figure 3b). It is evident that the real frequency dependence on k is close to the four-fluid (and therefore cold plasma) solution shown in Figure 1. This justifies the use of the four-fluid equations in the undamped or weakly damped solutions of the dispersion relation to estimate the fluid velocity components. The imaginary parts show the damping rate (negative growth rate).

[26] The long-dashes branch of the real frequency goes asymptotically to $\omega/\Omega_p = 1$ and is thus due to proton resonance. The corresponding imaginary part of this branch is negligible for $kC_A/\Omega_p < 1$. The short-dashed branch of the real frequency starts above the O^{6+} gyroresonant frequency ($\omega/\Omega_p = 6/16$) and goes asymptotically to the He^{++} resonant frequency ($\Omega/\omega_p = 0.5$). Calculation of the ion cyclotron resonance factors (the argument of the ζ function in equation (22) for each ion species, indicating resonance if the value is $\lesssim 3$ [*Gary et al.*, 1984]) shows that the corresponding damping rate is mostly due to the He^{++} resonance for $kC_A/\Omega_p \rightarrow 1$ and dominated by the O^{6+} resonance for $kC_A/\Omega_p \sim 0.5$. The solid line branch of the real frequency goes asymptotically to 6/16, with the

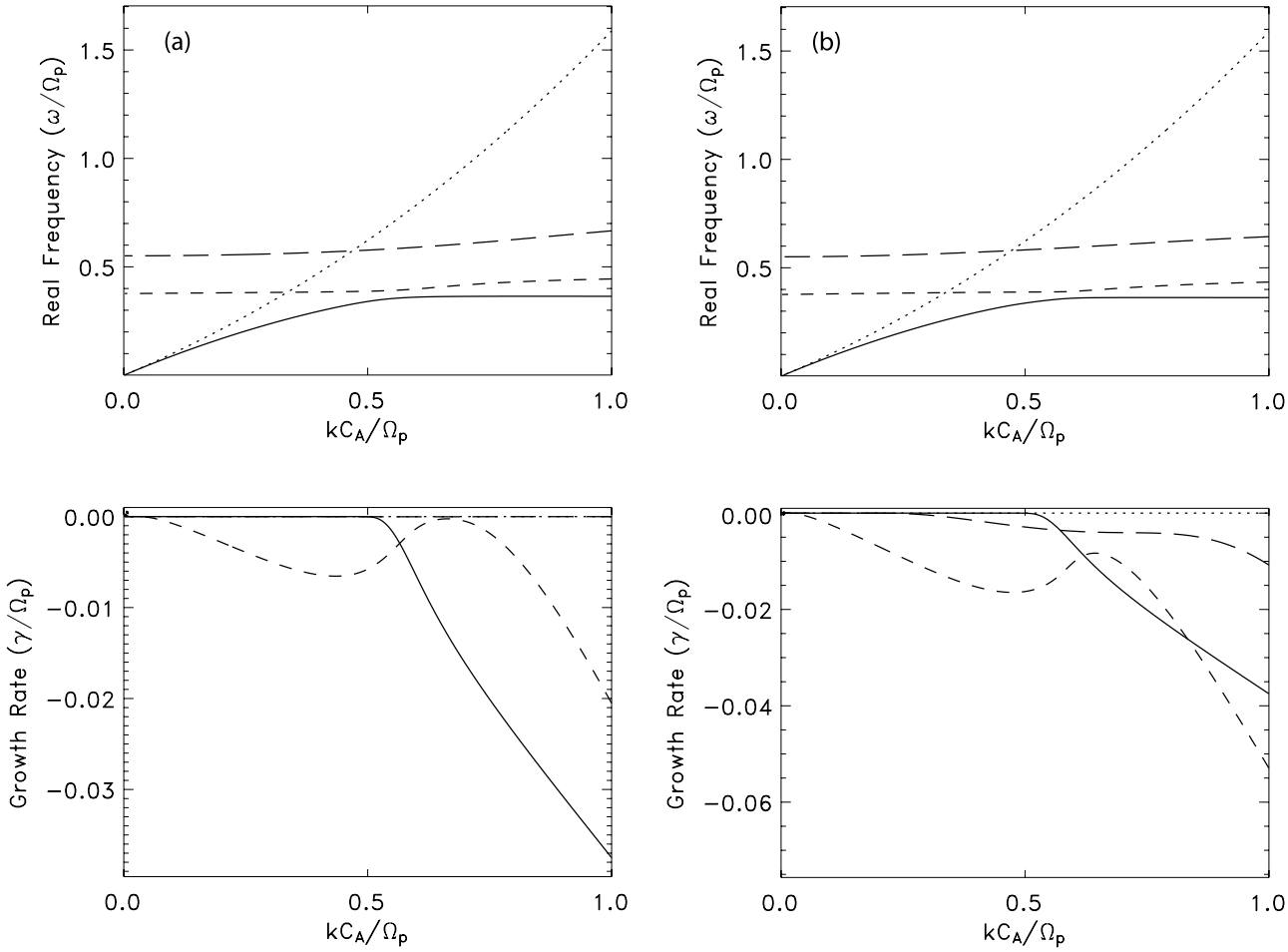

Figure 3. The solution of Vlasov's dispersion relation for warm plasma with protons, He^{++}, and O^{6+} ions. Top panels show the real part, and the bottom panels show the imaginary part of ω (i.e., damping rate). (a) β = 0.01; (b) β = 0.03.

corresponding resonant damping due to O^{6+}. The lower resonant branch (solid line) is nearly undamped below $kC_A/\Omega_p \approx 0.5$, and the middle resonant branch (short dashes) is weakly damped below $kC_A/\Omega_p \approx 1$, with minima at $kC_A/\Omega_p = 0$, and $kC_A/\Omega_p \approx 0.66$. The damping rate increases for all the resonant branches when β increases from 0.01 to 0.03. The nonresonant branch is not damped.

6. Hybrid Model Dispersion

[27] We use a one-dimensional hybrid code [e.g., *Winske and Omidi*, 1993] to model a collisionless, homogeneous, magnetized multispecies plasma. In the hybrid model the ions are represented as particles, while the electrons are described as a massless fluid to maintain quasi-neutrality of the plasma. The particle and field equations are integrated in time using a rational Runge-Kutta method, whereas the spatial derivatives are calculated by pseudospectral FFT method.

[28] In previous hybrid simulation studies, O^{5+} ions were included in multi-ion plasma with unrealistically large abundance due to the numerical difficulty to include the coronal abundance of O^{5+} [*Ofman et al.*, 2002; *Xie et al.*, 2004]. Here, the goal is to study the dispersion relation with coronal ion abundances, and we include the more abundant O^{6+} ions in addition to protons and He^{++} ions. The simulations were initialized with an isotropic Maxwellian velocity distributions for the ions, and an initial transverse magnetic field perturbation was imposed. We use a periodic system in z with the background magnetic field $\mathbf{B}_0 = \hat{z}\, B_0$ with 256 grid cells to solve for the fields, with 100 particles per cell for each component (i.e., 300 particles per cell, with the total of 76,800 particles) and with grid size $\Delta x = 1.5c/\omega_{pp}$. The integration time step was $\Omega_p \Delta t = 0.05$.

[29] Heating due to continuously driven wave spectrum was investigated previously [*Ofman et al.*, 2002; *Xie et al.*, 2004]. In the present study the wave spectrum was imposed in two steps: first, an f^{-1} spectrum of circularly polarized magnetic fluctuation with small amplitude ($\Delta B/B_0 = 0.01$) and in the frequency range $0.1-0.3\Omega_p$ was driven for $50\Omega_p^{-1}$ in a small region at the center of the simulated plasma (see detailed description of the driver in the work of *Ofman et al.* [2002] and *Xie et al.* [2004]). Next, the self-consistent (undriven) hybrid simulations were initialized using the results of the driven simulations as the initial state and run for about $1600\Omega_p^{-1}$. The dispersion relation was obtained by Fourier transforming the magnetic fluctuations and ion velocities in the second stage. During the first stage

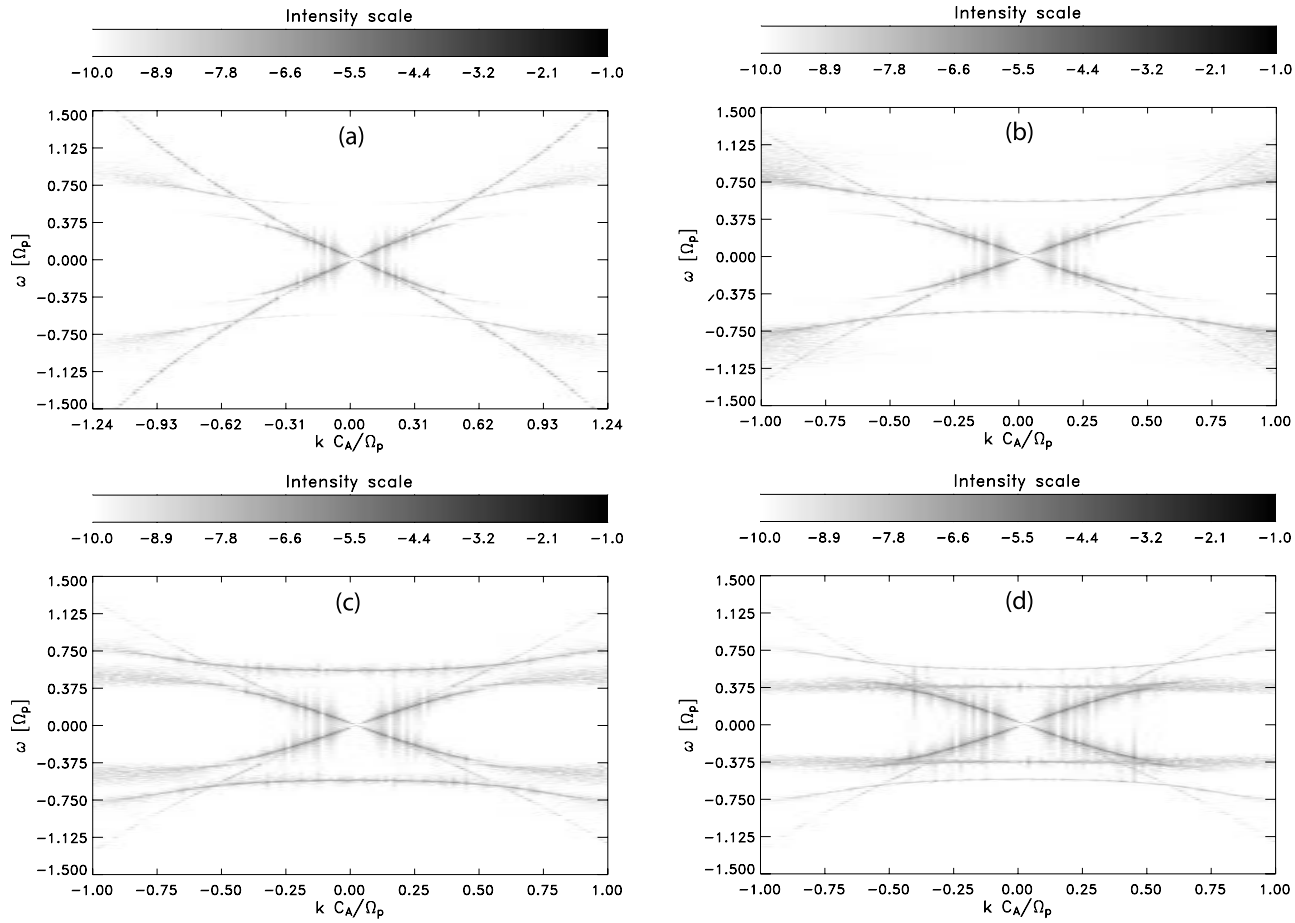

Figure 4. The dispersion relation of the proton-He^{++}-O^{6+} plasma is evident from the power of the Fourier transform in $\omega - k$ space of (a) transverse magnetic field fluctuations, $B_\perp$; transverse fluid velocities of the ions (b) $V_{\perp p}$; (c) $V_{\perp He^{++}}$; (d) $V_{\perp O^{6+}}$ calculated from the hybrid simulation model with coronal abundances of the ions and $\beta = 0.02$. Note the difference in the intensity of the resonant branches in each case. The dispersion branches agree with the four-fluid and Vlasov dispersion.

of the simulations, perpendicular heating has taken place in O^{6+}, increasing the temperature by 45%. Note that the resulting O^{6+} temperature anisotropy is stable in the low-β plasma and hence does not significantly affect the dispersion relation [*Ofman et al.*, 2001; *Gary et al.*, 2001]. The perpendicular heating of protons (2%) and of He^{++} (7%) was insignificant. In the second stage the perpendicular temperature has increased by 10% for O^{6+} and did not vary significantly for He^{++} and protons. The parallel thermal speed remains close to the initial value for $\beta = 0.02$. With $n_e = 10^8$ cm^{-3}, B = 5 G, and the corresponding $T = 1.4 \times 10^6$ K, we get the proton thermal speed 1.1×10^8 cm/s, the He^{++} thermal speed of 5.5×10^7 cm/s, and the O^{6+} thermal speed 2.7×10^7 cm/s.

[30] The dispersion relation of the proton-He^{++}-O^{6+} plasma shown in Figure 4 with the coronal abundances of the ions, and $\beta = 0.02$ was constructed as follows: the transverse magnetic field components ($B_\perp$) (Figure 4a) and the fluid velocity components of the ions ($V_\perp$) (Figures 4b–4d) were Fourier transformed both in space and time, and the modes were decomposed to modes with positive and negative helicity [*Terasawa et al.*, 1986]. The fluid velocity components in space-time were calculated by numerically integrating the moments of the velocity distributions of the protons and the heavy ions obtained from the hybrid simulations.

[31] The undamped and weakly damped parts of the dispersion branches are evident (here, all four quadrants in the $\omega - k$ space are shown). The branches are in good agreement with the four-fluid and Vlasov calculations of the dispersion relation. The right-hand polarized Alfvén wave branch extends throughout the Ω range. The lower left-hand polarized resonant branch approaches $\Omega_{O^{6+}}$ and is evident below $|kC_A/\Omega_p| \approx 0.5$. The weakly damped part of the middle left-hand polarized resonant branch is evident for $0.4 \lesssim kC_A/\Omega_p \lesssim 0.7$ in the magnetic field fluctuation and for the full range of k in the ion velocity fluctuations. The branch corresponds to the weakly damped region in the Vlasov dispersion relation (Figure 3). The normalized intensities of the branches are different for each ion velocity, $V_\perp i(\Omega, k)$. The intensities are consistent with the expected perpendicular fluid velocity ratios calculated from the multifluid cold plasma dispersion.

[32] In order to compare the hybrid simulation results with the four fluid results, we show in Figure 5 the ratio of the ion to protons fluid velocities as a function of ω for two

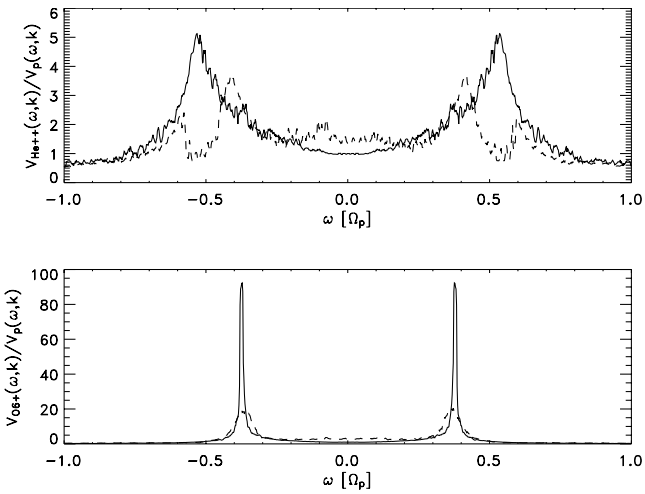

Figure 5. The ratio of the ion to protons velocities calculated from the hybrid model. The ratio $V_{He^{++}}/V_p$ is shown in the top panel for $kC_A/\Omega_p \approx 0$ (solid line) and for $kC_A/\Omega_p \approx 0.52$ (dashes). Bottom panel is the same as the top panel but for the ratio $V_{O^{6+}}/V_p$. Note, the good agreement with the values of the velocity ratios for the corresponding values of k calculated from the four-fluid theory, shown in Figure 2.

given values of k, calculated from the hybrid model run for about $3300\Omega_p^{-1}$ with the three ion species. To eliminate noise in the ratio due to the finite nature of the Fast Fourier Transform (FFT), the $\omega - k$ spectrum was smoothed over five points in the k grid space (where the k grid spacing is $\Delta k = 2\pi/L$, with $L = 256$ $\Delta z = 384c/\Omega_{pp}$). The ratio of the velocities in the Fourier space $V_{He^{++}}/V_p$ is shown in the top panel for $kC_A/\Omega_p \approx 0$ (solid line) and for $kC_A/\Omega_p \approx 0.52$ (dashes) and the ratio $V_{O^{6+}}/V_p$ for the same values of k is shown in the lower panel. The peaks of the velocity ratios are on the resonant branches of the dispersion. The approximate peak ratios of 100 and 20 for $V_{O^{6+}}/V_p$, and 3.5, and 5 for $V_{He^{++}}/V_p$ are in good agreement with the values of the velocity ratios for the corresponding k's on the resonant branches calculated from the four-fluid theory, shown in Figure 2. Thus the multifluid cold plasma velocity ratios are recovered in the fully nonlinear and self-consistent hybrid simulations of the warm multi-ion plasma.

7. Discussion and Conclusions

[33] We investigated the dispersion relation of Alfvén and ion-cyclotron waves in a multi-ion plasma using linearized multifluid cold plasma, Vlasov warm plasma, and nonlinear 1-D hybrid warm plasma models with coronal temperature and abundances of the He^{++} and O^{6+} ions. The advantages of the multifluid cold plasma model over kinetic description is the relative simplicity and the numerical tractability that allow to obtain global fluid quantities of each particle species for wave modes of interest. Since most observations of the corona are in minor ion emission lines, the multifluid cold plasma model is useful in the analysis of these observations. The main limitation of the multifluid cold plasma model is the lack of detailed information on the kinetic velocity distribution and the thermal damping effects. Therefore we have solved the linear Vlasov dispersion relation for warm multi-ion plasma and found good agreement with the four fluid cold plasma dispersion relation. The results were further confirmed with the hybrid simulation model of warm multi-ion plasma that is fully nonlinear and self-consistent. The main limitations of our models are the neglect of possible heavy ions drift relative to protons and the effects of possible temperature anisotropy in ion temperatures. Some aspects of these effects were investigated by previously using the 1-D hybrid model [*Ofman et al.*, 2002; *Xie et al.*, 2004].

[34] It is well known that in the presence of heavy ions the dispersion relation of the parallel propagating Alfvén cyclotron waves exhibits multiple branches: left-hand polarized resonant (due to each ion species) and right-hand polarized whistler branch. Using the multifluid cold plasma equations, we find the various relations between the ion and proton velocity amplitudes of each branch. The resonant branches results in high ion-to-proton velocity amplitude ratio. However, thermal effects limit the range of wavelengths that these branches can exist. For typical coronal temperatures and abundances the effect is strong for O^{6+} ions and significant for He^{++} ions for weakly damped wave numbers ($kC_A/\Omega_p \lesssim 1$).

[35] The contribution of the high-frequency waves to the observed ion emission line widths depends on the actual wave spectrum in the observed coronal structure and in particular on the power contained in the resonant branches. At present the exact spectrum of waves in the lower corona is unknown. Heliospheric observations beyond 0.3 AU by Helios show that the spectrum has a form of Ω^{-1} for frequencies below 10^{-4} Hz and $\Omega^{-5/3}$ for higher frequencies [e.g., *Grappin et al.*, 1990]. *Ofman and Davila* [2001] and *Ofman* [2004] have shown that the nonthermal motion of the protons due to the low-frequency waves can explain the observed hydrogen line broadening and that additional contribution of other processes is required to account for the heavy ion line broadening. We find that high-frequency Alfvén cyclotron waves can in principle account for the enhanced (compared with protons) minor ion nonthermal line broadening, and further, quantitative investigation of this effect on observed emission line widths of heavy ions is needed.

[36] In particular, we find that the resonant high-frequency (hybrid) branches of the dispersion relation can result in large unresolved wave motions that can lead to broad emission lines of He^{++} and O^{6+} compared with protons at the same temperature. Thus the observed line broadening of other heavy ions, such as O^{5+} may be the result of the averaged over the line-of-sight contribution of thermal and wave motions, with the high-frequency resonant waves contributing significantly to the line widths. Although the wave power spectrum may be concentrated in the low-frequency range, small fraction of that power at the heavy ion resonant frequencies can result in significantly enhanced average perpendicular ion velocities. The form of the unknown wave spectrum in various parts of the corona, the relative abundance of the heavy ions, the temperatures, and the local Alfvén and ion-cyclotron frequencies are the main factors that affect the nonthermal broadening of the emission lines due to this effect.

[37] Hybrid resonance waves have been observed for decades in the multi-ion space plasma of the ionosphere [*Smith and Brice*, 1964] and the magnetosphere in the past [*Young et al.*, 1981; *Fraser and McPherron*, 1982] and recently [e.g., *Mouikis et al.*, 2002]. In these observations it was found that the minor ions play a dramatic role in the modification of the electromagnetic ion cyclotron wave spectrum and that the minor ions can be strongly energized by the ion-cyclotron waves. Similarly, it is reasonable to assume that if ion cyclotron waves are present in the solar corona, then the heavy ions will strongly affect the ion-cyclotron wave spectrum. Several mechanism were proposed for the excitation of the hybrid resonance waves in the magnetosphere in the past [*Gendrin and Roux*, 1980; *Roux et al.*, 1982], and it is reasonable to assume that similar mechanisms may act in the solar coronal multi-ion plasma. For example, proton-cyclotron waves can be generated by a population of protons with temperature anisotropy ($T_\perp > T_\parallel$). The spectrum can interact resonantly and nonlinearly with the minor ions, generating the hybrid branches and eventually energizing the minor ions.

[38] **Acknowledgments.** LO would like to thank NASA grants NAG5-11877 and NNG04GA96G and NSF grant ATM-0135889.

[39] Shadia Rifai Habbal thanks S. Peter Gary and another referee for their assistance in evaluating this paper.

References

Araneda, J. A., A. F. Viñas, and H. F. Astudillo (2002), Proton core temperature effects on the relative drift and anisotropy evolution of the ion beam instability in the fast solar wind, *J. Geophys. Res.*, *107*(A12), 1453, doi:10.1029/2002JA009337.

Axford, W. I., and J. F. McKenzie (1992), The origin of high speed solar wind streams, in *Solar Wind Seven*, edited by E. Marsch and R. Schwenn, pp. 1–5, Elsevier, New York.

Cornwall, J. M., and M. Schulz (1971), Electromagnetic ion-cyclotron instabilities in multicomponent magnetospheric plasma, *J. Geophys. Res.*, *76*, 7791–7796.

Cranmer, S. R. (2000), Ion cyclotron wave dissipation in the solar corona: The summed effect of more than 2000 ion species, *Astrophys. J.*, *532*, 1197–1208.

Cranmer, S. R. (2002), Coronal holes and the high-speed solar wind, *Space. Sci. Rev.*, *101*, 229–294.

Cranmer, S. R., and A. A. van Ballegooijen (2003), Alfvénic turbulence in the extended solar corona: Kinetic effects and proton heating, *Astrophys. J.*, *594*, 573–591.

Cranmer, S. R., G. B. Field, and J. L. Kohl (1999), Spectroscopic constraints on models of ion cyclotron resonance heating in the polar solar corona and high-speed solar wind, *Astrophys. J.*, *518*, 937–947.

Cuperman, S., L. Gomberoff, and A. Sternlieb (1975), Requirements on singly ionized lithium concentrations for magnetospheric seeding experiments, *J. Geophys. Res.*, *80*, 4643–4647.

Cuperman, S., L. Ofman, and M. Dryer (1988), On the dispersion of ion cyclotron waves in H^+-He^{++} solar wind-like magnetized plasmas, *J. Geophys. Res.*, *93*, 2533–2538.

Davidson, R. C., and J. M. Ogden (1975), Electromagnetic ion cyclotron instability driven by ion energy anisotropy in high-beta plasmas, *Phys. Fluids*, *18*, 1045–1050.

Davila, J. M., R. J. Thomas, J. Brosius, and A. Poland (1997), The structure of the solar corona as observed by the Solar Extreme Ultraviolet Rocket Telescope and Spectrograph, *Adv. Space Res.*, *20*, 2293–2298.

Dmitruk, P., W. H. Matthaeus, L. J. Milano, S. Oughton, G. P. Zank, and D. J. Mullan (2002), Coronal heating distribution due to low-frequency, wave-driven turbulence, *Astrophys. J.*, *575*, 571–577.

Dusenbery, P. B., and J. V. Hollweg (1981), Ion-cyclotron heating and acceleration of solar wind minor ions, *J. Geophys. Res.*, *86*, 153–164.

Fraser, B. J., and R. L. McPherron (1982), Pc 1–2 magnetic pulsation spectra and heavy ion effects at synchronous orbit - ATS 6 results, *J. Geophys. Res.*, *87*, 4560–4566.

Fried, B. D., and S. D. Conte (1961), *The Plasma Dispersion Function*, Elsevier, New York.

Gary, S. P. (1978), Ion-acoustic-like instabilities in the solar wind, *J. Geophys. Res.*, *83*, 2504–2510.

Gary, S. P. (1993), *Theory of Space Plasma Microinstabilities*, Cambridge Univ. Press, New York.

Gary, S. P., D. W. Forslund, C. W. Smith, M. A. Lee, and M. L. Goldstein (1984), Electromagnetic ion beam instabilities, *Phys. Fluids*, *27*, 1852–1862.

Gary, S. P., L. Yin, D. Winske, and L. Ofman (2001), Electromagnetic heavy ion cyclotron instability: Anisotropy constraint in the solar corona, *J. Geophys. Res.*, *106*, 10,715–10,722.

Gendrin, R., and A. Roux (1980), Energization of helium ions by proton-induced hydromagnetic waves, *J. Geophys. Res.*, *85*, 4577–4586.

Gomberoff, L., and R. Elgueta (1991), Resonant acceleration of alpha particles by ion cyclotron waves in the solar wind, *J. Geophys. Res.*, *96*, 9801–9804.

Grappin, R., A. Mangeney, and E. Marsch (1990), On the origin of solar wind MHD turbulence: Helios data revisited, *J. Geophys. Res.*, *95*, 8197–8209.

Hara, H., and K. Ichimoto (1999), Microscopic nonthermal plasma motions of coronal loops in a solar active region, *Astrophys. J.*, *513*, 969–982.

Harrison, R. A., et al. (1995), The coronal diagnostic spectrometer for the Solar and Heliospheric Observatory, *Sol. Phys.*, *162*, 233–290.

Hassler, D. M., G. J. Rottman, E. C. Shoub, and T. E. Holzer (1990), Line broadening of MG X 609 and 625 A coronal emission lines observed above the solar limb, *Astrophys. J.*, *348*, L77–L80.

Hollweg, J. V., and P. A. Isenberg (2002), Generation of the fast solar wind: A review with emphasis on the resonant cyclotron interaction, *J. Geophys. Res.*, *107*(A7), 1147, doi:10.1029/2001JA000270.

Isenberg, P. A. (1984), The ion cyclotron dispersion relation in a proton-alpha solar wind, *J. Geophys. Res.*, *89*, 2133–2141.

Isenberg, P. A. (2004), The kinetic shell model of coronal heating and acceleration by ion cyclotron waves: 3. The proton halo and dispersive waves, *J. Geophys. Res.*, *109*, A03101, doi:10.1029/2002JA009449.

Isenberg, P. A., and J. V. Hollweg (1982), Finite amplitude Alfven waves in a multi-ion plasma - Propagation, acceleration, and heating, *J. Geophys. Res.*, *87*, 5023–5029.

Kohl, J. L., and G. L. Withbroe (1982), EUV spectroscopic plasma diagnostics for the solar wind acceleration region, *Astrophys. J.*, *256*, 263–270.

Kohl, J. L., et al. (1995), The Ultraviolet Coronagraph Spectrometer for the Solar and Heliospheric Observatory, *Solar Phys.*, *162*, 313–356.

Kohl, J. L., et al. (1997), First results from the SOHO Ultraviolet Coronagraph Spectrometer, *Solar Phys.*, *175*, 613–644.

Kohl, J. L., et al. (1998), UVCS/SOHO empirical determinations of anisotropic velocity distributions in the solar corona, *Astrophys. J.*, *501*, L127–L131.

Li, B., X. Li, Y. Hu, and S. R. Habbal (2004), A two-dimensional Alfvén wave-driven solar wind model with proton temperature anisotropy, *J. Geophys. Res.*, *109*, A07103, doi:10.1029/2003JA010313.

Li, X. (2003), Transition region, coronal heating and the fast solar wind, *Astron. Astrophys.*, *406*, 345–356.

Li, X., S. R. Habbal, J. Kohl, and G. Noci (1998), The Effect of temperature anisotropy on observations of Doppler dimming and pumping in the inner corona, *Astrophys. J.*, *501*, L133–L137.

Marsch, E. (1999), Cyclotron heating of the solar corona, *Astrophys. Space Sci.*, *264*, 63–76.

Marsch, E., and C.-Y. Tu (1997), The effects of high-frequency Alfven waves on coronal heating and solar wind acceleration., *Astron. Astrophys.*, *319*, L17–L20.

McKenzie, J. F., and E. Marsch (1982), Resonant wave acceleration of minor ions in the solar wind, *Astrophys. Sp. Sci.*, *81*, 295–314.

Mouikis, C. G., et al. (2002), Equator-S observations of He^+ energization by EMIC waves in the dawnside equatorial magnetosphere, *Geophys. Res. Lett.*, *29*(10), 1432, doi:10.1029/2001GL013899.

Nakariakov, V. M., L. Ofman, and T. D. Arber (2000), Nonlinear dissipative spherical Alfvén waves in solar coronal holes, *Astron. Astrophys.*, *353*, 741–748.

Narain, U., P. Agarwal, R. K. Sharma, L. Prasad, and B. N. Dwivedi (2001), On coronal loop heating by torsional Alfvén waves, *Solar Phys.*, *199*, 307–315.

Neupert, W. M., G. L. Epstein, R. J. Thomas, and W. T. Thompson (1992), An EUV imaging spectrograph for high-resolution observations of the solar corona, *Solar Phys.*, *137*, 87–104.

Ofman, L. (2004), Three-fluid model of the heating and acceleration of the fast solar wind, *J. Geophys. Res.*, *109*, A07102, doi:10.1029/2003JA010221.

Ofman, L., and J. M. Davila (1997), Do first results from SOHO UVCS indicate that the solar wind is accelerated by solitary waves?, *Astrophys. J.*, *476*, L51–L54.

Ofman, L., and J. M. Davila (1998), Solar wind acceleration by large-amplitude nonlinear waves: Parametric study, *J. Geophys. Res.*, *103*, 23,677–23,690.

Ofman, L., and J. M. Davila (2001), Three-fluid 2.5-dimensional magnetohydrodynamic model of the effective temperature in coronal holes, *Astrophys. J.*, *553*, 935–940.

Ofman, L., A. Viñas, and S. P. Gary (2001), Constraints on the O^{+5} anisotropy in the solar corona, *Astrophys. J.*, *547*, L175–L178.

Ofman, L., S. P. Gary, and A. Viñas (2002), Resonant heating and acceleration of ions in coronal holes driven by cyclotron resonant spectra, *J. Geophys. Res.*, *107*(A12), 1461, doi:10.1029/2002JA009432.

O'Shea, E., D. Banerjee, and S. Poedts (2003), Variation Of coronal line widths on and off the disk, *Astron. Astrophys.*, *400*, 1065–1070.

Pekünlü, E. R., Z. Bozkurt, M. Afsar, E. Soydugan, and F. Soydugan (2002), Alfvén waves in the inner polar coronal hole, *Mon. Not. R. Astron. Soc.*, *336*, 1195–1200.

Roux, A., S. Perraut, J. L. Rauch, C. de Villedary, G. Kremser, A. Korth, and D. T. Young (1982), Wave-particle interactions near omega He^{+} observed on board GEOS 1 and 2:2. Generation of ion cyclotron waves and heating of He^{+} ions, *J. Geophys. Res.*, *87*, 8174–8190.

Scharer, J. E., and A. W. Trivelpiece (1967), Cyclotron wave instabilities in a plasma, *Phys. Fluids*, *10*(3), 591–595.

Smith, R. L., and N. Brice (1964), Propagation in multicomponent plasmas, *J. Geophys. Res.*, *69*, 5029–5040.

Stix, T. H. (1992), *Waves in Plasmas*, Springer, New York.

Terasawa, T., M. Hoshino, J. Sakai, and T. Hada (1986), Decay instability of finite amplitude circularly polarized Alfvén waves: A numerical simulation of stimulated Brillouin scattering, *J. Geophys. Res.*, *91*, 4171–4187.

Tu, C.-Y., and E. Marsch (1997), Two-fluid model for heating of the solar corona and acceleration of the solar wind by high-frequency Alfven waves, *Solar Phys.*, *171*, 363–391.

Vainio, R., T. Laitinen, and H. Fichtner (2003), A simple analytical expression for the power spectrum of cascading Alfvén waves in the solar wind, *Astron. Astrophys.*, *407*, 713–723.

Wilhelm, K., et al. (1995), SUMER - Solar Ultraviolet Measurements of Emitted Radiation, *Solar Phys.*, *162*, 189–231.

Wimmer-Schweingruber, R. F., R. von Steiger, J. Geiss, G. Gloeckler, F. M. Ipavich, and B. Wilken (1998), O5+ in High Speed Solar Wind Streams: SWICS/Ulysses Results, *Space Sci. Rev.*, *85*, 387–396.

Winske, D., and N. Omidi (1993), *Computer Space Plasma Physics: Simulation Techniques and Sowftware*, edited by H. Matsumoto and Y. Omura, pp. 103–160, Terra Sci., Tokyo.

Withbroe, G. L., J. L. Kohl, H. Weiser, and R. H. Munro (1982), Probing the solar wind acceleration region using spectroscopic techniques, *Space Sci. Rev.*, *33*, 17–52.

Xie, H., L. Ofman, and A. Viñas (2004), Multiple ions resonant heating and acceleration by Alfvén/cyclotron fluctuations in the corona and the solar wind, *J. Geophys. Res.*, *109*, A08103, doi:10.1029/2004JA010501.

Young, D. T., S. Perraut, A. Roux, C. de Villedary, R. Gendrin, A. Korth, G. Kremser, and D. Jones (1981), Wave-particle interactions near Omega/He^{+} observed on GEOS 1 and 2. I - Propagation of ion cyclotron waves in He^{+}-rich plasma, *J. Geophys. Res.*, *86*, 6755–6772.

J. M. Davila and L. Ofman, NASA Goddard Space Flight Center, Code 612.1, Greenbelt, MD 20771, USA. (joseph.m.davila@nasa.gov; leon.ofman@gsfc.nasa.gov)

V. M. Nakariakov, Physics Department, University of Warwick, Coventry, CV4 7AL, UK. (v.nakariakov@warwick.ac.uk)

A.-F. Viñas, NASA Goddard Space Flight Center, Code 612.2, Greenbelt, MD 20771, USA. (adolfo.vinas@gsfc.nasa.gov)